IAEA nuclear fusion

PAPER • OPEN ACCESS

TRANSP-TGLF core predictive modeling of the JET DT baseline scenario

OPEN ACCESS
IOP Publishing | International Atomic Energy Agency

Nuclear Fusion

Nucl. Fusion **66** (2026) 056043 (14pp)

https://doi.org/10.1088/1741-4326/ae5de2

TRANSP-TGLF core predictive modeling of the JET DT baseline scenario

F. Auriemma[1,2,*], Hyun-Tae Kim[3], J. Lombardo[2,4], R. Lorenzini[2,5], S. Gabriellini[3], L. Garzotti[3], V.K. Zotta[6], D. Frigione[7], S. Menmuir[3], M. Gorelenkova[8], A.Y. Pankin[8], F. Rimini[3], G.M. Staebler[9,10], Ž. Štancar[3], D. Van Eester[9,10], J. Garcia[11], J. Hillesheim[3], P. Lomas[3], C. Lowry[3], JET Contributors[a] and the EUROfusion Tokamak Exploitation Team[b]

[1] ISTP, CNR, C.so Stati Uniti 4, 35127 Padova, Italy
[2] Consorzio RFX, CNR, ENEA, INFN, UNIPD, Acciaierie Venete SpA, C.so Stati Uniti 4, 35127 Padova, Italy
[3] United Kingdom Atomic Energy Authority, Culham Campus, Abingdon OX13 3DB, United Kingdom of Great Britain and Northern Ireland
[4] Centro Ricerche Fusione—Università a di Padova, Padova, Italy
[5] ENEA-Centro Ricerche Bologna, Bologna, Italy
[6] Dipartimento di Ingegneria, Astronomia, Elettronica ed Energia, Sapienza University of Rome, v. Eudossiana 18, 00184 Roma, Italy
[7] Tor Vergata University of Roma, Via del Politecnico 1, Roma, Italy
[8] Princeton Plasma Physics Laboratory, Princeton, NJ 08543-0451, United States of America
[9] General Atomic, PO Box 85608, San Diego, CA 92121, United States of America
[10] Laboratory for Plasma Physics LPP-ERM/KMS, B-1000 Brussels, Belgium
[11] CEA, IRFM, F-13108 Saint-Paul-lez-Durance, France

E-mail: fulvio.auriemma@igi.cnr.it

Received 21 January 2026, revised 12 March 2026
Accepted for publication 10 April 2026
Published 30 April 2026

Abstract

In recent years, an intense modeling activity has been focused on preparing and analyzing the second JET Deuterium–Tritium (D–T) experimental campaign DTE2. Among the numerous scientific outcomes of this campaign was the unique opportunity to test and validate the state of the art of modeling tools with fusion-relevant DT plasmas using the full metallic ITER-like wall in different scenarios. This work reports on the core predictive modeling of plasma density, electron and ion temperatures (n_e, T_e, T_i) performed using TRANSP (Pankin *et al* 2025 *Comput. Phys. Commun.* **312** 109611) coupled with Trapped Gyro-Landau Fluid (TGLF)-SAT2 (Kinsey *et al* 2008 *Phys. Plasmas* **15** 055908), (Staebler *et al* 2021 *Nucl. Fusion* **61** 116007) for the JET D–T baseline scenario ($I_p = 3.5$ MA, $q_{95} = 3$, $\beta_N < 2$, with pellet pacing) (Garzotti *et al* 2025 *Plasma Phys. Control. Fusion* **67** 075011). The sensitivity to different input parameters, as the $\vec{E} \times \vec{B}$ shear parameterization and the values of the kinetic quantities at the boundary of the prediction domain ($\rho = 0.85$) has been assessed, identifying the confidence interval of the

[a] See Maggi *et al* 2024 (https://doi.org/10.1088/1741-4326/ad3e16) for JET Contributors.
[b] See Joffrin *et al* 2024 (https://doi.org/10.1088/1741-4326/ad2be4) for the EUROfusion Tokamak Exploitation Team.
* Author to whom any correspondence should be addressed.

prediction results. In particular, the dependence of the electron density profile on the particle source parameters has been studied, identifying the ionization source as the main cause for the density gradient under-prediction obtained by TRANSP-TGLF, reported in (Hyun-Tae *et al* 2023 *Nucl. Fusion* **63** 112004).

Keywords: JET, transport, plasma performance, TRANSP, TGLF-SAT2, predictive modelling, baseline scenario

(Some figures may appear in colour only in the online journal)

1. Introduction

Reliable prediction of Deuterium–Tritium (DT) plasma performance in term of fusion power is crucial for designing and optimizing DT operational scenarios in present and future fusion devices. However, such prediction remains a challenging task, as fusion power is highly sensitive to plasma kinetic profiles, which depend on phenomena developing on different spatial and temporal scales. The DT fusion reaction rate increases more than linearly with fuel ion density and temperature, requiring advanced integrated modeling that accurately reproduces plasma heating and transport processes. To achieve trustworthy predictive capability, it is essential to quantitatively assess existing modeling tools against experimental data and to identify areas for improvement [1]. Additionally, in ITER [2] a robust preparation of the nuclear phase of the machine will be based on the preliminary operation in pure deuterium. The assessment of the performance dependence on the plasma isotope composition, along with the uncertainties on the measured plasma parameters is a key topic to obtain reliable information from the modeling prediction.

The recent DTE2 JET campaign [3] provides the ideal test-bed to tackle this challenge and quantify the accuracy of simulated DT fusion power against actual measurements [4]. Indeed in such campaign sustained plasma operation in reactor relevant condition, where DT fusion power has been produced for many confinement times, has been routinely obtained in different plasma scenarios.

A large predictive modeling activity, based on the result of the DTE2 campaign, has been already performed as reported in [5]. In such paper the prediction capabilities of the most used transport codes in the fusion community are discussed. Besides the numerous results presented, it emerges that an evident underestimate of the predicted density (and density gradient) were present in the results obtained by a part of the numerical codes involved in the comparison.

This work primarily investigates the causes of the modeled under-prediction, focusing on the best-performing pure deuterium and DT baseline discharges [6] obtained during the preparation and execution of the DTE2 campaign, namely pulses 96 482 and 99 948. The analysis has been performed using the TRANSP [7] code, coupled with the Trapped Gyro-Landau Fluid (TGLF) [8, 9] quasilinear turbulent transport model.

As a second objective, the study quantifies the confidence intervals of the predicted performance by means of a sensitivity analysis on the main plasma parameters, identifying the most relevant quantities and mechanism affecting fusion performance. The comparison of the responses of deuterium and DT plasmas to such parameter scan, demonstrates that D and DT baseline plasmas exhibit similar trends.

1.1. Structure of the paper

After the general introduction to provide the relevant background information in section 1, the results of the TRANSP-TGLF prediction of the core kinetic profiles for the best performing pure D and D–T mixture baseline pulses of DTE2, respectively 96 482 and 99 948, are presented in section 2. Section 3 investigates the possible causes for the mismatch between the experimental and modeling results, identifying the correct particle source settings to match the experimental density gradient. The sensitivity to the main simulation parameters are reported in section 4, where a discussion about the effect of the boundary condition on the plasma transport properties and on the computed neutron rate is presented, comparing the trends obtained by the D and the DT pulses. Section 5 summarizes the main findings and reports on the conclusion of the work.

2. Prediction results of D baseline pulse 96 482 and DT counterpart 99 948

The highest neutron rate of the baseline scenario developed in JET with Deuterium as main gas (some percent of Hydrogen as minority specie is also injected) has been obtained in pulse 96 482, at 3.5 MA of plasma current, auxiliary input power $P_{\mathrm{NBI+PICRH}} = 29.0 + 4.5\,\mathrm{MW}$, with D pellet ELM pacing. Similar engineering parameters have been used in the DTE2 JET campaign, with the aim of achieving high performance baseline plasma sustained for 5 s. The best results have been obtained with pulse 99 948 which, by the way, has been stopped by high Z (mainly W) impurity accumulation after about 2.5 s of the high performance phase [6]. Indeed the reduced ELM frequency featured by the DT plasma despite the injected ELM pacing pellets, leads to the lack of tungsten flushing, with the consequent radiation increase on the low field side that causes the plasma termination at 51.4 s.

Figure 1 reports the time traces of the main discharge parameters: plasma current, toroidal field, NBI and ICRH additional power results very well matched between the 2 pulses, as well as the temperatures and line integral density (with only a slight density increase in the DT pulse). As stated, the DT pulse ends with a disruption at about 51.4 s. Nevertheless, the

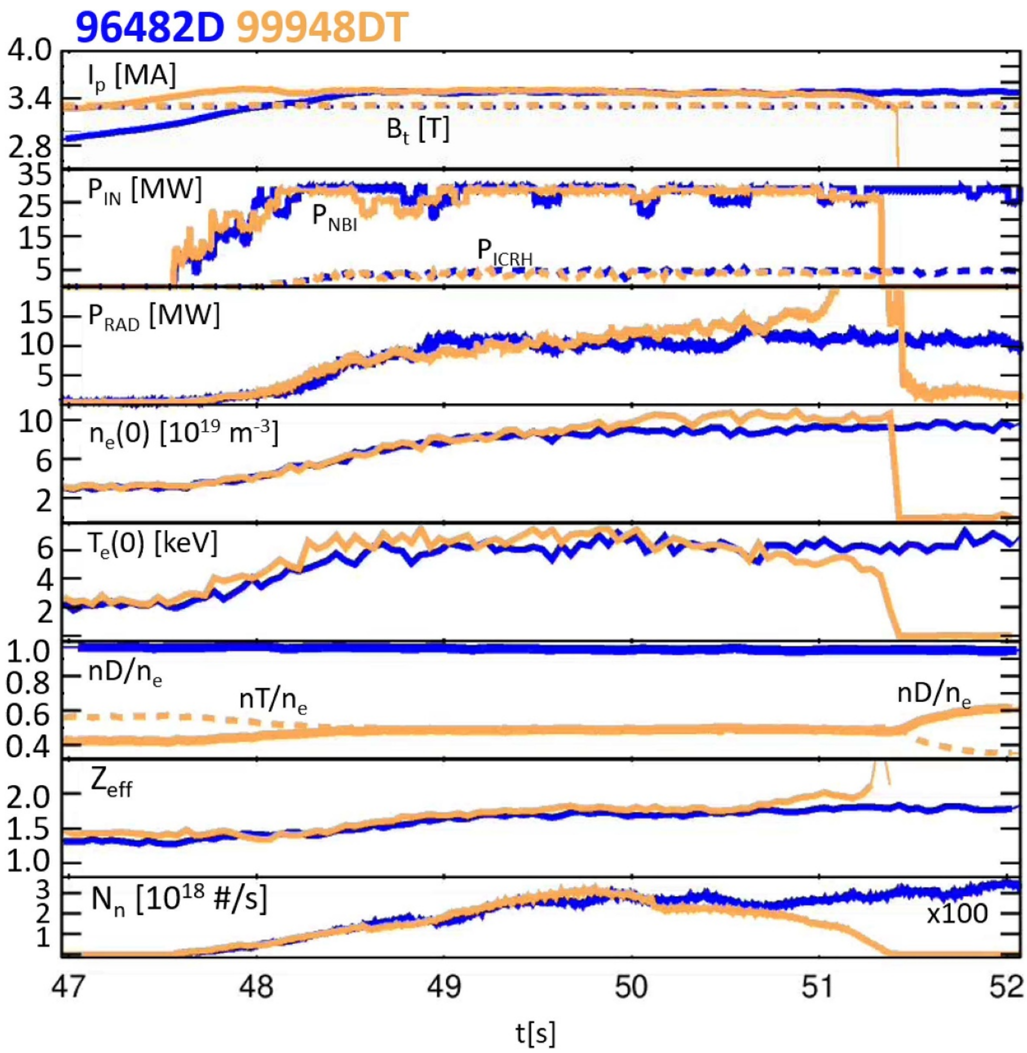

Figure 1. Comparison of the time traces of the most relevant plasma parameters for pure Deuterium pulse 96 482, in blue, and Deuterium–Tritium mixture one 99 948, in orange. From top to bottom, the plasma current I_p and the toroidal field B_t; the additional power (NBI solid line, ICRH dashed line); the radiated power P_{rad}; the core electron density $n_e(0)$ and temperature $T_e(0)$; the hydrogenic isotope concentration; the effective charge Z_{eff}; and the neutron rate N_n (x100 in the D case).

steady phase is long enough to use this pulses to test and validate the predictive capability of TRANSP-TGLF.

In [5] the n_e, T_e and T_i profiles are predicted under the same settings and assumptions by different transport codes and compared with the experimental results, both for the pure D and for the DT plasmas. The main assumptions includes the prescribed pedestal profiles in $\rho_t = [0.85;1]$ ($\rho_t = \sqrt{\Psi_t} = \sqrt{\frac{\tilde{\Psi}_t}{\tilde{\Psi}_t|_{sep}}}$ is the squared root of the normalized toroidal flux Ψ_t defined as the ratio of the flux of the magnetic toroidal field $\tilde{\Psi}_t$ over its value at the separatrix $\tilde{\Psi}_t|_{sep}$), while the rotation and radiation profiles are prescribed on the whole radius. The Z effective value is taken from the experiment, and 1% Be and Ni, whose concentration is computed to match the prescribed Z effective, are imposed. In the predictive simulation, no W is included. This assumption is justified by the fact that the radiation profile, which affects the electron power balance, is prescribed whereas the W contribution to the plasma Z effective is negligible because of its small concentration in the time window of interest: [50.0–50.5] s for the D pulse and [49.5–50.0] s for the DT one. The radiation profile is computed as the flux surface average of the 2D poloidal bolometric reconstruction. The equilibrium is computed with the fixed boundary TRANSP internal solver, imposing the shape of the last closed flux surface and the edge safety factor, while evolving the plasma current profile. As for the transport model, TGLF-SAT2 including perpendicular magnetic fluctuations is used, the main ion density is computed in TRANSP via quasi-neutrality (considering both impurities and α particle densities) and no ad-hoc electromagnetic stabilization model (i.e. EM_STAB = 0) has been activated. The list of the main TGLF-SAT2 settings is reported in table A1. These settings have been applied to all the predictive simulations presented in this paper, to allow an easier, direct comparison of the results.

Under such assumptions, three channels TRANSP-TGLF(SAT2) predictive simulations are performed in the radial domain $\rho_t = [0;0.85]$. Figure 2 shows the predicted profiles averaged in the steady state of the plasma: [50.0–50.5] s

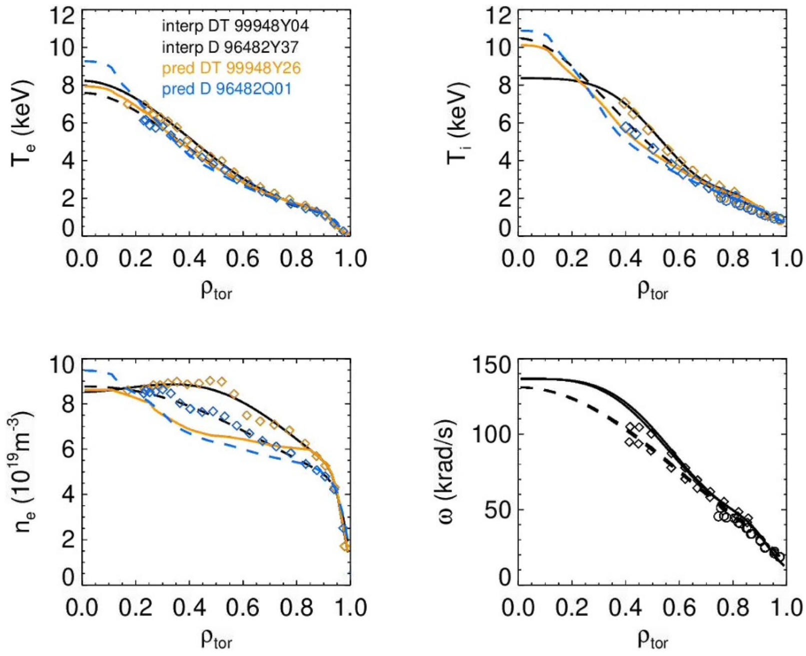

Figure 2. Comparison of the predicted radial profiles of electron density, electron temperature, ion temperature for the deuterium pulse 96 482, in blue, and the Deuterium–Tritium pulse 99 948, in orange. The black profiles represent the fit of the experimental data (empty diamonds), the solid line refers to DT pulse and the dashed one to the D pulse. The plasma rotation frequency is interpretive.

and [49.5–50.0] s for D and DT pulse, respectively. In the same figure, the experimental data (diamonds) and the corresponding fitted profiles are reported (black lines). The predicted electron temperature is in good agreement with the high resolution Thomson scattering (HRTS) [10, 11] data in $\rho_t = [0.25; 0.85]$. Differences between predicted and fitted profiles can be observed at $\rho_t < 0.25$, where they can be neglected because no experimental data are available to constrain the fits. The same behavior is obtained also for the the predicted ion temperature, whose profile aligns well with the experimental Ti data, for both D and DT cases.

On the contrary, the density prediction results underestimated, with a density gradient in the region $\rho_t = [0.5, 0.85]$ extremely flat and in disagreement with the measured density gradient for both D and DT plasmas [12]. A proper quantification of the discrepancy between predicted profiles and experimental data is reported in section 3.3 and figure 8.

The lower plasma density lead to a computed neutron rate 17% lower than the experimental one in the DT case and, similarly, 23% lower in the D pulse.

To understand the reasons for the under-predicted density, different routes have been explored: (1) the presence of a possible problem in the interface between TRANSP and TGLF; (2) the dependence of the electro-magnetic turbulence stabilization on the $\vec{E} \times \vec{B}$ shear parameterization and magnitude; (3) the effect of the particle source on the density gradient in the region $\rho_t = [0.5; 0.85]$

3. Possible causes for the density under-prediction

Before investigating any potential physical cause which leads to the electron density underprediction, we checked that there was no issue in the interface between the TRANSP code and the TGLF transport model. The test methodology and its results are described in the following paragraph.

3.1. TRANSP-TGLF interface

TRANSP evolves the n_e profile solving the particle continuity equation at each time step:

$$\frac{\partial n_e(\rho_t, t)}{\partial t} = \frac{1}{V'}\left[-\nabla \cdot \Gamma(\rho_t, t)\right] + S(\rho_t, t) \tag{1}$$

where Γ is the particle flux and S is the particle source term, ρ_t and t are the radial and temporal coordinates, reported to highlights that such quantities vary in time and position. The particle fluxes are computed by TGLF, the particle sources from the neutral beam are computed by the NUBEAM [13] code, which is a widely used and benchmarked Monte Carlo code for NBI heating, fueling, torque injection, and current drive. The wall and recycling source are provided as input data and their propagation towards the core are computed by the FRANTIC [14] code. The workflow used in this study does not allow a detailed modeling of the pellet injection physics and a simplified approach described in section 3.3 has been used.

The equation (1) is solved at several radial points in the prediction domain. To obtain the Γ, TGLF read in the plasma parameters from the TRANSP simulation, as the local electron, ion and fast ion densities and temperature, the $\vec{E} \times \vec{B}$ shear, the geometry of the flux surface, etc. The particle flux computed by TGLF is then passed back to TRANSP. At each time step and at each radial point, all such information are saved in temporary files (the so-called dump files), which

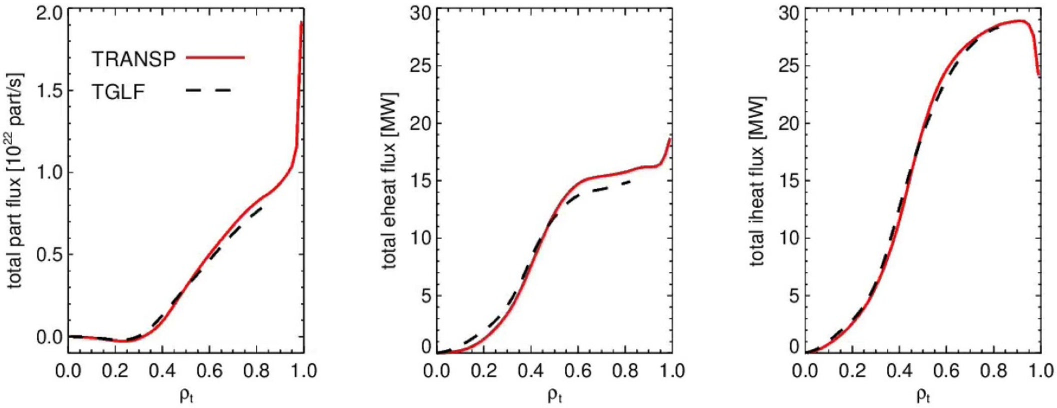

Figure 3. Comparison of the particle, electron heat, and ion heat fluxes computed by TGLF (dashed black line) and TRANSP (solid red line) at the first time step of the simulation for pulse 96 482. In the region $\rho_t = [0 - 0.85]$ the fluxes results in agreement.

are usually overwritten at the following time step. To verify that the interface between the two codes is properly working, we stopped the TRANSP run after the first TGLF call, in order to have the predictive particle, and electron and ion heat fluxes used in TRANSP to be compared with the corresponding quantities in the TGLF dump files. Since TRANSP does not save the particle, electron and ion heat fluxes, but only their divergence (first term of the right-hand side of equation (1)), the fluxes are computed starting from the TRANSP output variables. The particle flux is hence obtained as:

$$\Gamma(\rho_t) = \Sigma_{\text{irad}=0}^{\text{NRAD}} \left(\text{EPTR\_MOD(irad)} \times \text{DVOL(irad)}\right) \quad (2)$$

at each time step. EPTR_MOD is the divergence of the particle flux and DVOL is the volume of each zone in the TRANSP radial grid, based on NRAD points. The heat fluxes are similarly computed, with the variables EETR_MOD and IETR_MOD, for electrons and ions, respectively.

The comparison of the TRANSP and TGLF fluxes is reported in figure 3 for the 3 channels: the red solid line represent the $\Gamma(\rho_t, t)$ in TRANSP whereas the dashed line is the same quantity extracted from TGLF dump files, resulting in very good agreement. Note that the TGLF computation is done only in the integration domain $\rho_t = [0, 0.85]$ and, correctly, no information on the pedestal particle flux, where TGLF is not valid, are provided to TRANSP.

This simple but mandatory test rules out any possible issue in the interface of the 2 codes, and confirms that TRANSP is actually using the fluxes computed by TGLF on the base of the plasma parameters of the previous time step.

3.2. *Turbulence stabilization by $\vec{E} \times \vec{B}$ shear*

The sheared $\vec{E} \times \vec{B}$ velocity $v_{\vec{E}\times\vec{B}} = \vec{E} \times \vec{B}/B^2 \sim E_r/B_t$, where E_r is the radial component of the electric field and B_t is the toroidal component of the magnetic field, can play a crucial role in suppressing the electromagnetic turbulence. Its proper computation is a key factor to recover a good agreement between modeled and experimental profiles. In a plasma, radial force balance yields an equation for radial electric field E_r [15, 16]:

$$E_r(\rho_t, t) = -\frac{\nabla P}{e n_e} - v_t B_p + v_p B_t \quad (3)$$

where the first term, the diamagnetic one, is related to the gradient of the plasma pressure (∇P), e is the elementary charge and n_e is the electron density. The second and the third terms are, respectively, the product of the toroidal velocity v_t by the poloidal magnetic field B_p and the poloidal velocity v_p by the toroidal magnetic field B_t.

TGLF requires in input the local sheared $v_{\vec{E}\times\vec{B}}$ velocity, the so-called $\vec{E} \times \vec{B}$ shear $\tilde{\gamma}_E$, which is computed as [16]:

$$\tilde{\gamma}_E = \frac{r}{q}\frac{\mathrm{d}}{\mathrm{d}r}\left(\frac{E_r}{RB_p}\right) = -\frac{r}{q}\frac{\mathrm{d}}{\mathrm{d}r}\left(\frac{v_t B_p}{RB_p}\right) \quad (4)$$

where the radial electric field is computed neglecting the pressure gradient and the $v_p B_t$ terms (i.e. $E_r = -v_t B_p$). The safety factor q and the plasma major radius R enter the formula with their common definitions.

To verify that the $\tilde{\gamma}_E$ definition required by TGLF is valid in the parameter space of the discharges under analysis, we compute the contribution of each term in the E_r definition, as reported in figure 4. In such figure the adimensional $\tilde{\gamma}_E$ is shown, multiplying it by the constant factor a/c_S, where a is the plasma minor radius and c_S is sonic velocity.

It turns out that, in the region with $\rho_t < 0.85$, the $\tilde{\gamma}_E$ computed with the $v_t B_p$ term only accounts for the 95% of the total $\vec{E} \times \vec{B}$ shear, as shown in figure 4(*a*). The contribution of the pressure gradient term is significative only in the pedestal region, while the $v_p B_t$ term has negligible amplitude everywhere, confirming that the definition used is sound in the radial domain under analysis. We also checked that the $\tilde{\gamma}_E$ computed by TRANSP correctly uses the equation (4) and that TGLF actually receives such values in input. To do this additional check, the TGLF dumps files have been compared with the TRANSP internally computed $\vec{E} \times \vec{B}$ and with the same quantity manually computed: the 3 lines results in optimal agreement, as shown in figure 4(*b*).

To assess the sensitivity to the $\vec{E} \times \vec{B}$ shear of the turbulent fluxes, a scan with different values of $\tilde{\gamma}_E$ has been performed. Figure 5 reports the results of such test on the predicted kinetic quantities. The scan has been done applying a

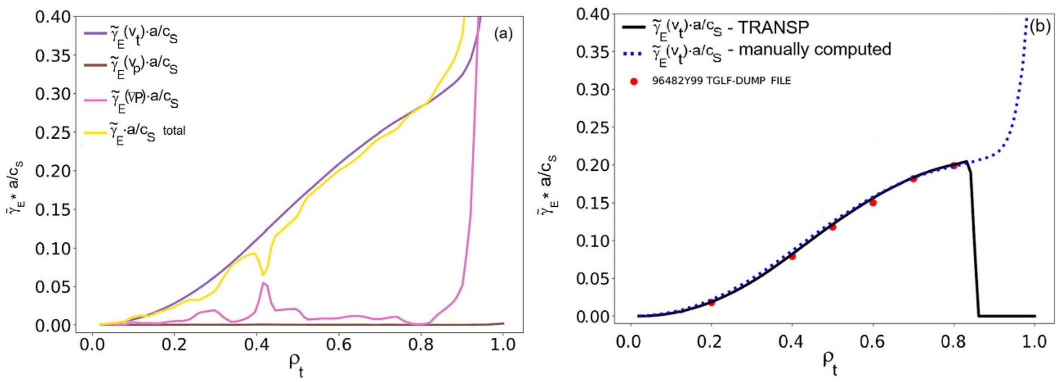

Figure 4. (*a*) Normalized $\vec{E}\times\vec{B}$ shear rate components computed in TRANSP: in purple the E_r is computed as $-(v_t B_p)$; in brown as $(v_p B_t)$; in pink as $-(\frac{\nabla P}{e n_e})$. The dominant term in the region $\rho_t < 0.85$ turns out to be the purple one, which is comparable with the total $\vec{E}\times\vec{B}$, in solid yellow line. (*b*) $\vec{E}\times\vec{B}$ taken at the first time step of a TRANSP simulation for pulse 96 482 (solid black line), compared with the same quantity computed following the equation (4) with the toroidal velocity component only (blue dotted line). The red full dots represent the input provided to TGLF by TRANSP, to be used in the computation of the particle and heat fluxes.

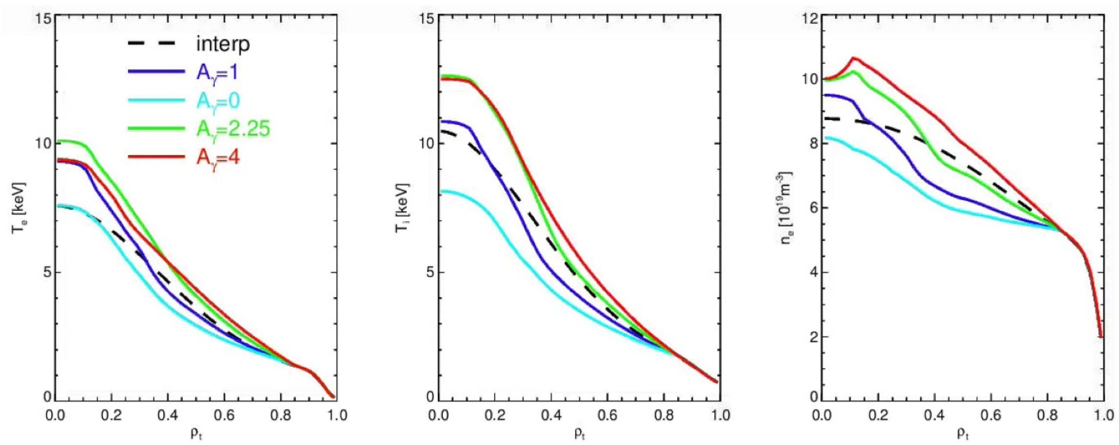

Figure 5. Predicted kinetic profiles for pulse 96 482 obtained scanning the $\vec{E}\times\vec{B}$ shear rate, compared with the interpretive simulation in dashed black line, used as a proxy of the experimental profiles.

multiplying factor A_γ to the $\tilde{\gamma}_E$ in each simulation in the range $[0, 1, 2.25, 4]$. Switching off the $\vec{E}\times\vec{B}$ stabilization results in a even flatter n_e profile in the region $\rho_t = [0.5; 0.85]$, with a general underestimate of all the predicted quantities. The increase of A_γ to 2.25 provides a good agreement of the density profile with the experimental data, but the core T_i and the full T_e profile are overestimated. In particular the T_e profile turns out to be not compatible with the measurements of the HRTS. $A_\gamma = 4$ produces a too strong turbulence stabilization on all channels, with all the profiles largely over-predicted.

The main outcome is that the factor $A_\gamma = 2.25$, which recovers a reasonable agreement of the computed density profile with the experimental data, cannot be applied on the temperatures channels. Additionally such an increase of the $\tilde{\gamma}_E$ is not justified by the error bars of the toroidal velocity as measured by the charge exchange radiation monitor, either.

3.3. Particle source

Given that the turbulent transport fluxes in TRANSP are consistent with the TGLF output, according to equation (1), the remaining knob to affect the density profile, is the particle source $S(\rho_t, t)$. The detailed study of the particle sources, which involves pedestal and boundary physics not included in the present modeling, is beyond the scope of this work. Nevertheless, a simple but effective approach is used: the gas fueling, wall recycling, and pellet injection, which are all sources of particles present in the JET baseline plasmas, are modeled as a single effective source S_{eff}, which is then scaled to predict the outer core density gradient $\left.\frac{\mathrm{d}n_e}{\mathrm{d}\rho}\right|_{0.85}$ close to the experimental one. It is important to note that the value of the source at the boundary condition is a critical parameter for the solution of the differential equation (1). The NBI particle source is self-consistently computed by NUBEAM, with default settings and no anomalous fast ion diffusion. The $S_{\mathrm{eff}}(\rho_t, t)$ is computed by FRANTIC, where the free parameters are the neutral temperature at the edge $T_n(1)$ which determines the incoming neutral velocity, and the separatrix neutral density.

The results are shown in figure 6, where the predicted density profiles (*b*) of discharge 96 482 averaged between 10.0 s

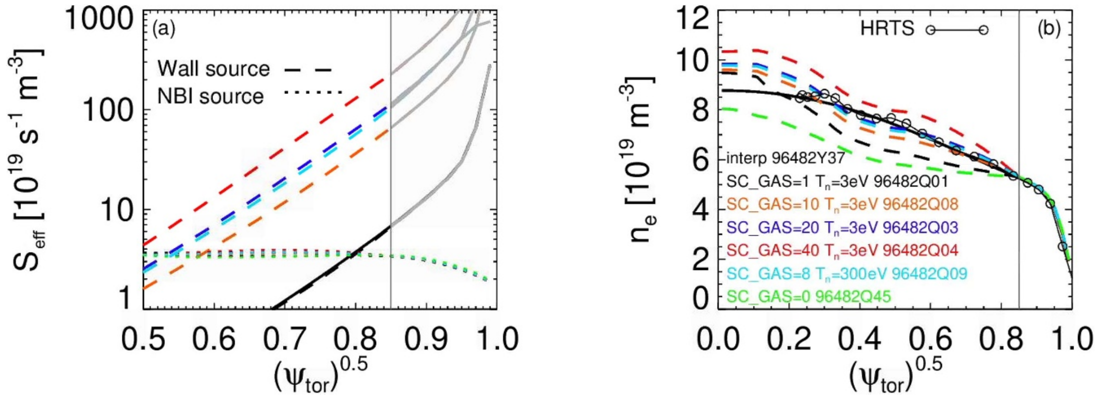

Figure 6. (*a*) Effective wall particle source S_{eff} for different SC_{GAS} and $T_{\mathrm{n}}(1)$ combinations. The NBI fueling is reported in the dotted line, for comparison. (*b*) Corresponding electron density predicted profiles. To match the HRTS data (empty dots), the particle source shall be about 15 times larger than $S_{\mathrm{eff}}(0.85)$ provided by the nominal gas injection system (black lines).

and 10.5 s are shown for different particle sources (*a*). The panel (*a*) reports also the particle source provided by NBI, which results almost unaffected by the change in the effective wall source settings. In the increased S_{eff} cases the wall and the NBI sources becomes comparable at $\rho_{\mathrm{t}} \approx 0.5$. The increased S_{eff} results in a steeper density gradient in the core's outer region, which propagates towards the center. The optimal value of $S_{\mathrm{eff}}(0.85)$ turns out to be about 15 times larger than the source provided by only the gas injection system. Such value can be obtained by simply multiplying the puffing neutral density by a scaling factor SC_{GAS} and/or modifying the neutral atoms' edge temperature $T_{\mathrm{n}}(1)$ to increase their penetration depth. Different combinations of neutral scaling factor and $T_{\mathrm{n}}(1)$ result in similar $S_{\mathrm{eff}}(0.85)$: the dark blue and light blue dashed lines represent the cases ($SC_{\mathrm{GAS}} = 20, T_{\mathrm{n}}(1) = 3\,\mathrm{eV}$), and ($SC_{\mathrm{GAS}} = 8, T_{\mathrm{n}}(1) = 300\,\mathrm{eV}$), respectively. The latter edge neutral temperature can be interpreted as the average energy between the molecule dissociation energy (3 eV) provided by the gas puffing valves and the backscattering neutral energy which is in the order of the edge ion temperature. A similar value ($T_{\mathrm{n}}(1) \approx 300\,\mathrm{eV}$) is also found in the integrated core-edge-SOL simulations performed in similar pulses with JINTRAC-COCONUT [17] and references therein. As an additional test, a simulation without any particle source has been performed . The result is a even flatter density profile, not far from what obtained with ($SC_{\mathrm{GAS}} = 1, T_{\mathrm{n}}(1) = 3\,\mathrm{eV}$), suggesting and confirming that such settings are unlikely to correctly represent the effective particle source.

To provide an independent verification of the effective particle source computed with the discussed simplified model, a full radius JINTRAC-TGLF [18] predictive simulation of pulse 96 482 has been performed [19]. In such simulation the boundary condition for the electron density profile is put at $\rho = 1$. The total particle source is simulated by JINTRAC including the particles provided by the gas valves system, the pellet injector, the wall recycling, and the NBI contribution given by PENCIL. The pedestal transport properties have been set in order to reproduce the experimental density pedestal height and width, exploiting the heuristic pedestal transport model [19], assuming a $\chi/D = 4$ (ratio of the heat diffusivity over the particle diffusivity) in the pedestal.

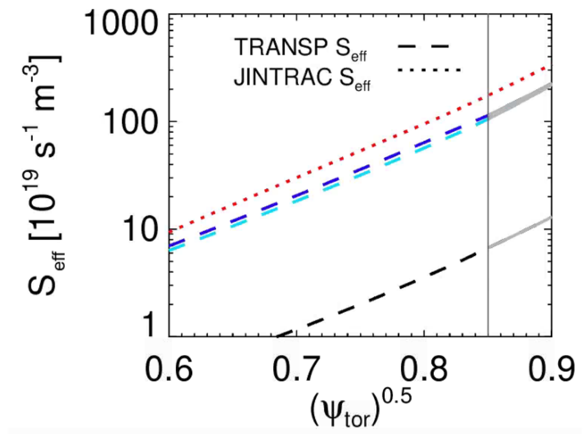

Figure 7. Total particle source (removing the NBI contribution) computed by JINTRAC in the full radius simulation (black solid line) compared with the S_{eff} used in TRANSP runs with $SC_{\mathrm{GAS}} = 20, T_{\mathrm{n}}(1) = 3\,\mathrm{eV}$ (dark blue dashed) and $SC_{\mathrm{GAS}} = 8, T_{\mathrm{n}}(1) = 300\,\mathrm{eV}$ (ligh blue dashed).

The particle core transport has been computed by TGLF from the top of the pedestal to the magnetic axis. The comparison of the total particle source computed by JINTRAC with the S_{eff} shown in figure 6 confirms that the optimal settings for the effective particle source are ($SC_{\mathrm{GAS}} = 20, T_{\mathrm{n}}(1) = 3\,\mathrm{eV}$), and ($SC_{\mathrm{GAS}} = 8, T_{\mathrm{n}}(1) = 300\,\mathrm{eV}$). Figure 7 shows the comparison of the total particle source computed by JINTRAC with the 2 TRANSP optimal cases and with the reference case ($SC_{\mathrm{GAS}} = 1, T_{\mathrm{n}}(1) = 3\,\mathrm{eV}$), confirming that the particle source used in [5] is not sufficient to sustain the density gradient in the region $\rho = [0.4 - 0.85]$.

The TRANSP-TGLF, predictive analysis for the DT discharge 99 948 shows similar features, with ion and electron temperature well-matched and under-predicted n_{e}. The same approach is hence used to study the behavior of the DT discharge.

It turns out that an enhancement of the particle source of the same order of magnitude is required to correctly match the experimental data. Since the modified electron density affects also the prediction of the temperature, generally resulting in lower temperatures when the density increases,

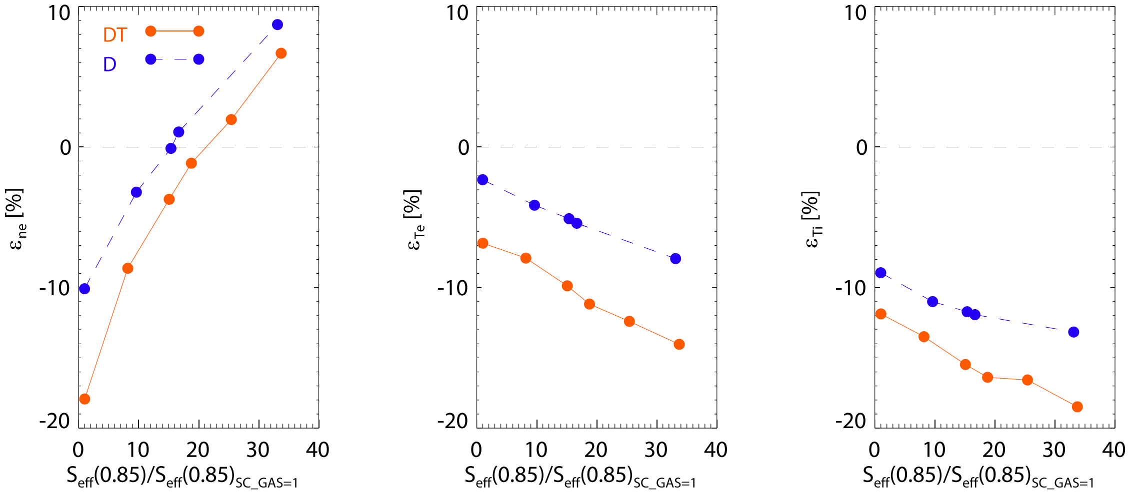

Figure 8. Relative discrepancy of the density (*a*), electron temperature (*b*), and ion temperature (*c*) as a function of the particle source at $\rho_t = 0.85$ normalized to the source obtained with $SC_{\mathrm{GAS}} = 1, T_n(1) = 3$ at the same position (boundary of the integration region). The Orange color refers to DT pulse, the blue one to the D case.

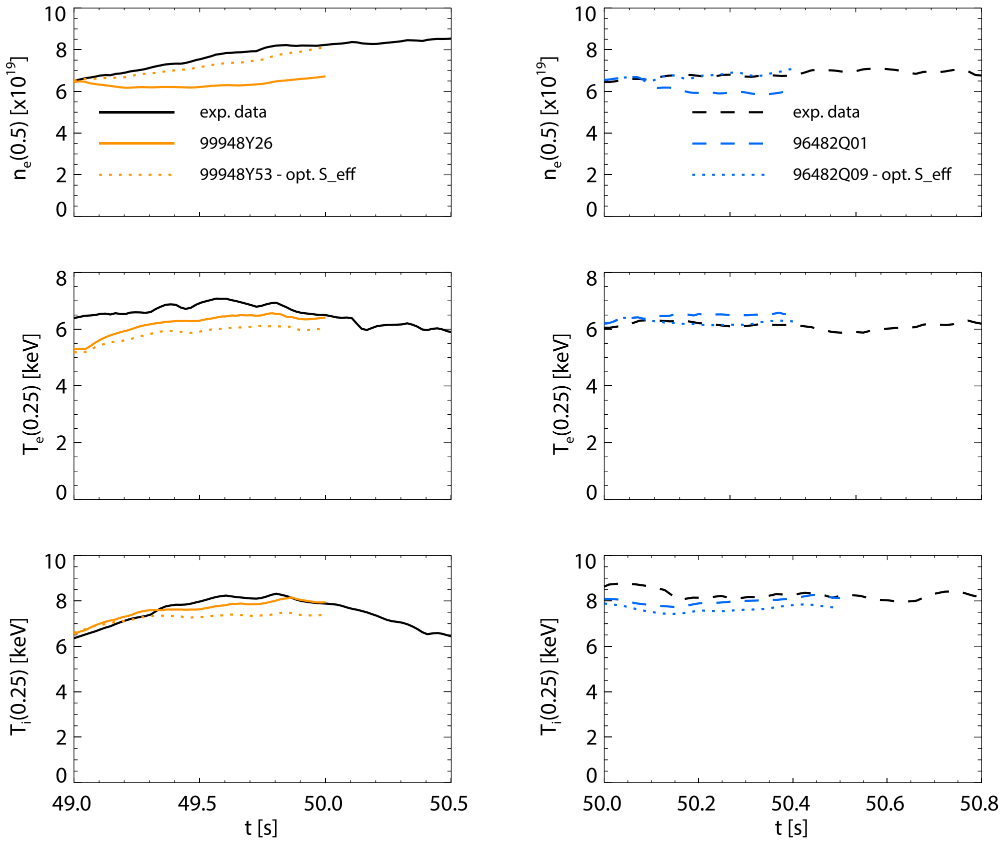

Figure 9. Electron density at mid radius, core electron temperature, core ion temperature time-traces for D pulse 96 482 (right column) and for the DT pulse 99 948 (left column). The experimental measurement are in black lines, whereas the predicted quantities are in dotted line for the simulation with optimized particle source ($T_n(1) = 300\,\mathrm{eV}, SC_{\mathrm{GAS}} = 9$) and in solid orange and dashed blue for the case with low particle source ($T_n(1) = 3\,\mathrm{eV}, SC_{\mathrm{GAS}} = 1$), used in previous work.

an estimate of the discrepancy for the different particle source parameters is provided. Figure 8 reports $S_{\mathrm{eff}}(0.85)$ normalized to the value obtained with $(SC_{\mathrm{GAS}} = 1, T_n = 3\,\mathrm{eV})$ and the corresponding average discrepancy $\varepsilon_{x_{\mathrm{mod}}} = \frac{1}{\mathrm{NRAD1}} \sum_{\rho=0.25}^{\rho=0.85} \left(\frac{x_{\mathrm{mod}} - x_{\mathrm{exp}}}{x_{\mathrm{exp}}}\right)$ between the experimental quantities $x_{\mathrm{exp}} = (n_e, T_e, T_i)$ and the corresponding modeled one x_{mod} (NRAD1 is the number of radial points in [0.25, 0.85]). In both the D and DT discharges, the electron density prediction shows a variation of ε_{n_e} larger than 20%, with a minimum at $\frac{S_{\mathrm{eff}}(0.85)}{S_{\mathrm{eff}}(0.85)_{SC_{\mathrm{GAS}}=1}} \approx 15 - 18$ (see panel (*a*)). The T_e and

Table 1. Summary table of the sensitivity test of the plasma performance to the main plasma parameters. $\varepsilon_N = -12\%$ for the DT pulse, $\varepsilon_N = -14\%$ for the D pulse.

	Factor (−)	DT ε_N	D ε_N	Factor (+)	DT ε_N	D ε_N
Pedestal T_i	0.9	−24%	−23%	1.1	−3%	−3%
Pedestal T_e	0.9	−14%	−11%	1.1	−16%	−15%
Pedestal n_e	0.9	−16%	−18%	1.1	−13%	−10%
Z effective	0.9	−16%	−16%	1.2	−9%	−10%
Angular frequency	0.8	−16%	−17%	1.2	−9%	−
Rotation shear	0.8	−18%	−20%	1.2	−8%	−7%

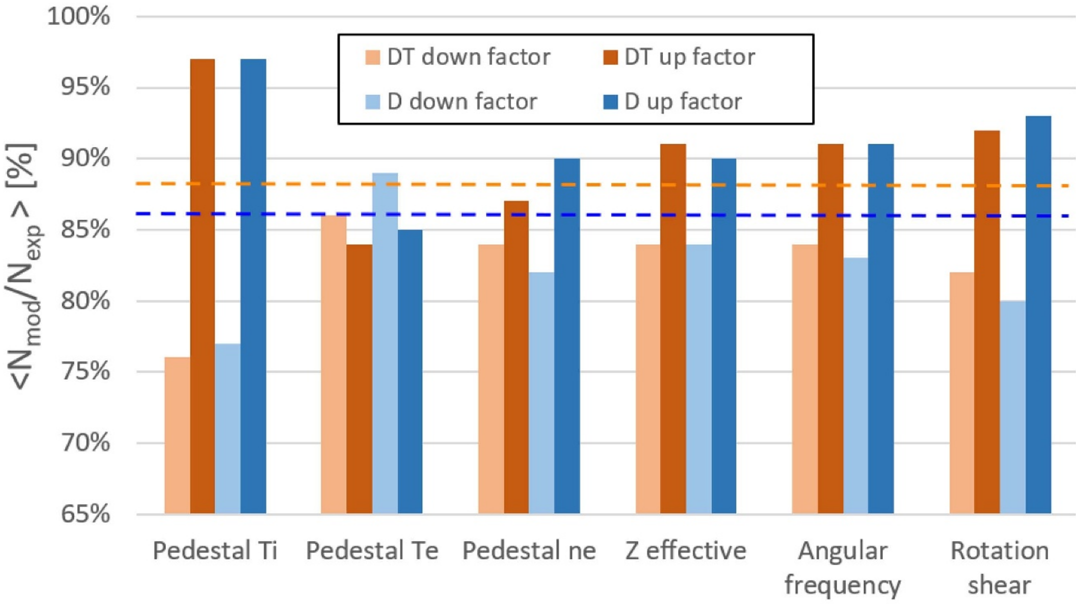

Figure 10. Graphic representation of the sensitivity test of the plasma performance to the main plasma parameters. Light blue and dark blue refer to D pulse 96 482, light orange and dark orange refer to DT pulse 99 948, the lighter color indicates the neutron discrepancy resulted reducing the parameters under investigation, the darker color shows the results obtained increased the same parameter, for each category. The dashed lines represent the discrepancy level for both the DT (orange) and D (blue) pulses. The comparison between D and DT results confirm how the response of the neutron production to the parameter scan is weak, in this regime.

T_i prediction are much less affected by the particle source scan, with a maximum variation of ε_{T_e} and ε_{T_i} below 7%, as reported in panels (*b*) and (*c*).

To properly evaluate the capability of the TRANSP-TGLF(SAT2) simulations of capturing the time evolution of the predicted plasma quantities, the time-traces of the experimental electron density at mid radius, of the core electron and ion temperatures are compared with the corresponding predicted quantities. Figure 9 reports, from top to bottom, the experimental $n_e(\rho_t = 0.5, t)$, the $T_e(0.25, t)$ and $T_i(0.25, t)$ in black line. The orange solid and blue dashed in each plot represent the same quantities for the case $(T_n(1) = 3\,\mathrm{eV}, SC_{GAS} = 1)$, whereas the dotted orange and blue lines are the results of the corresponding simulations performed with the optimized S_{eff}. Specifically they are obtained setting $(T_n(1) = 300\,\mathrm{eV}, SC_{GAS} = 9)$. In both D (blue) and DT (orange) cases, a better agreement of the time evolution of the electron density is observed while minor effects on the temperatures are found.

Estimating the confinement properties from the described simulation, a synergistic effect is observed: increasing the particle source, a larger density is obtained which damps the electromagnetic turbulence. Indeed the confinement time increases by a factor 6–10 with the enhanced S_{eff}. Additionally, the magnitude of the particle source estimated in this works turns out to be consistent with independent studies [20, 21].

The overall modeling agreement with the experimental total neutron rate N_{Nexp} results $\varepsilon_N = \frac{N_{Nmod} - N_{Nexp}}{N_{Nexp}} = -12\%$ at its best, being N_{Nmod} the modeled neutron rate. The residual difference is mainly due to the T_i uncertainties, and its response to the increased density. Additionally ε_{T_e} goes from −7% to −11%, which reduces the fast ion population and hence the total neutron rate via the beam-target channel. A sensitivity test on the main experimental inputs has been performed within the experimental uncertainties to evaluate their impact on the plasma performance prediction.

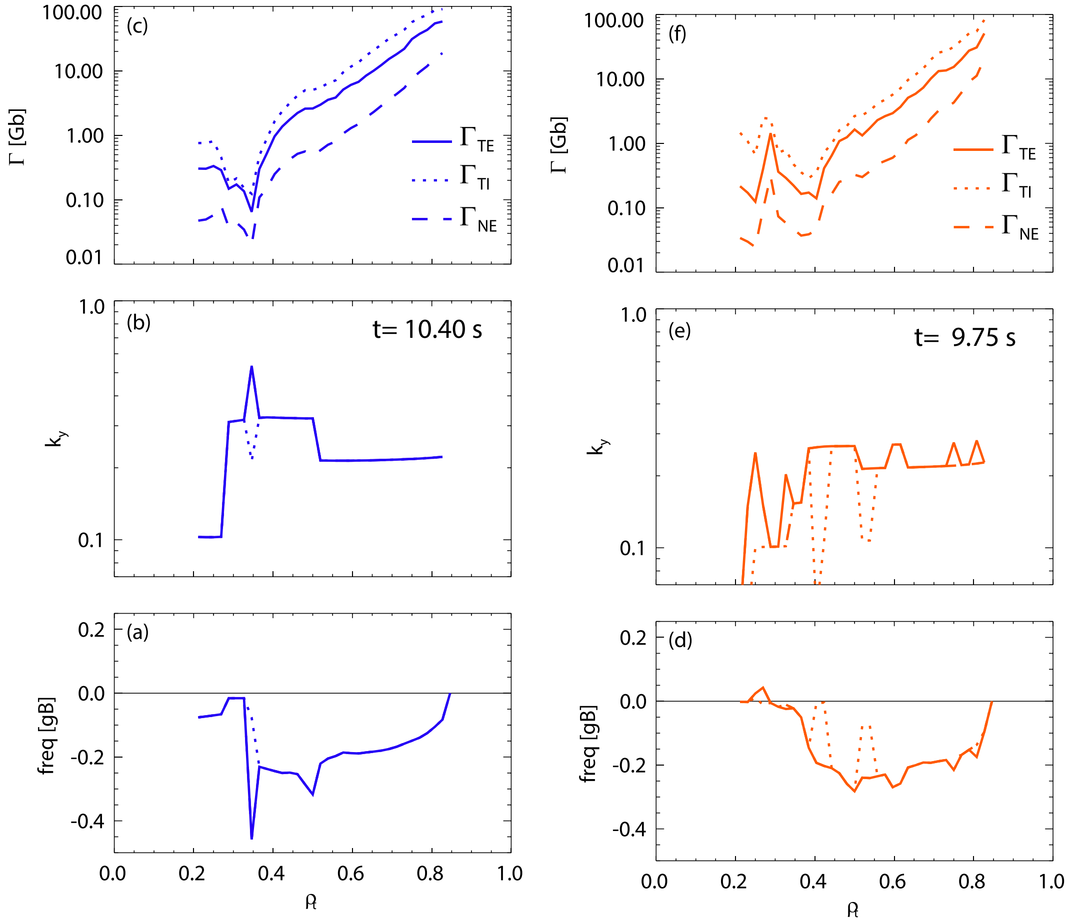

Figure 11. (*a*) and (*d*): radial profiles of the maximum quasi-linear flux for heat (T_e solid, T_i dotted) and particle (n_e dashed) computed by TGLF in D simulation 96 482Q09 (left column) and DT run 99 948Y53 (right column), where the optimized S_{eff} is applied. (*b*) and (*e*) show the wavenumber k_y corresponding to the maximum flux for each location and the associated frequency in gyroBohm units.

4. Sensitivity test of the modeling results for D and D–T baseline pulses

The modeling results are sensitive to quantities that affect the turbulent transport, such as main ion dilution, T_i/T_e, rotation profile, $\vec{E}\times\vec{B}$ shear, q profile, and magnetic shear. Moreover also the boundary conditions at the integration domain modify the outcome of the computation. To test how these quantities affect the prediction of the total neutron rate in both D and DT plasmas, a $\pm10\%$ on pedestal value of T_i, T_e, n_e have been applied, considering this as a good estimate of their average measurement error bars or experimental uncertainties. The variation on Z effective is -10% $+20\%$ and the interval for the rotation profiles is $\pm20\%$: the core CX measurements are affected by a larger error than the pedestal ones due to a lower signal to noise ratio, and the Z effective measurement at JET is affected by a similar error in the last DTE2 campaign. The non-symmetric Z effective variation interval is chosen to avoid values below 1. Additionally, to test the sensitivity to the core rotation velocity and its shear, a factor that goes linearly from 1 at $\rho_t = 1$ to 1.2 (or 0.8) on the magnetic axis has been applied to the angular frequency data.

Table 1 reports the results of the sensitivity scans which are also graphically summarized in figure 10, where for each tested variation, the corresponding agreement between the modeled and the experimental neutron rate is shown. In general the results for D and DT plasmas are similar: such outcome shows that the propagation of the input parameters uncertainties on the predicted fusion performance, in particular on the neutron rate, is similar in D and DT plasmas for this experimental condition.

To have a better understanding of the behavior shown in table 1 and figure 10, the dominant turbulence mechanism has been investigated. Figures 11(*a*) and (*d*) show, for D and DT case respectively, the radial profiles of the maximum quasi-linear fluxes for each channel, computed by TGLF in $\rho_t = [0.25, 0.85]$. The corresponding k_y (*b*) and (*d*) and the associated frequency (*c*) and (*f*). These plasmas result dominated by low wavenumber fluctuation with negative frequency, which corresponds to the so-called ion temperature gradient (ITG) turbulence. No dominant mode are reported in the high k_y range, suggesting that the Electron Temperature Gradient turbulence is a sub-dominant drive of heat and particle transport. The dominant ITG turbulence for the JET plasmas is consistent with previous detailed gyrokinetic analysis [22, 23].

Considering the ITG nature of the transport in these plasmas, the strongest dependence of the fusion performance on the T_i can be attributed to synergistic effects. The higher

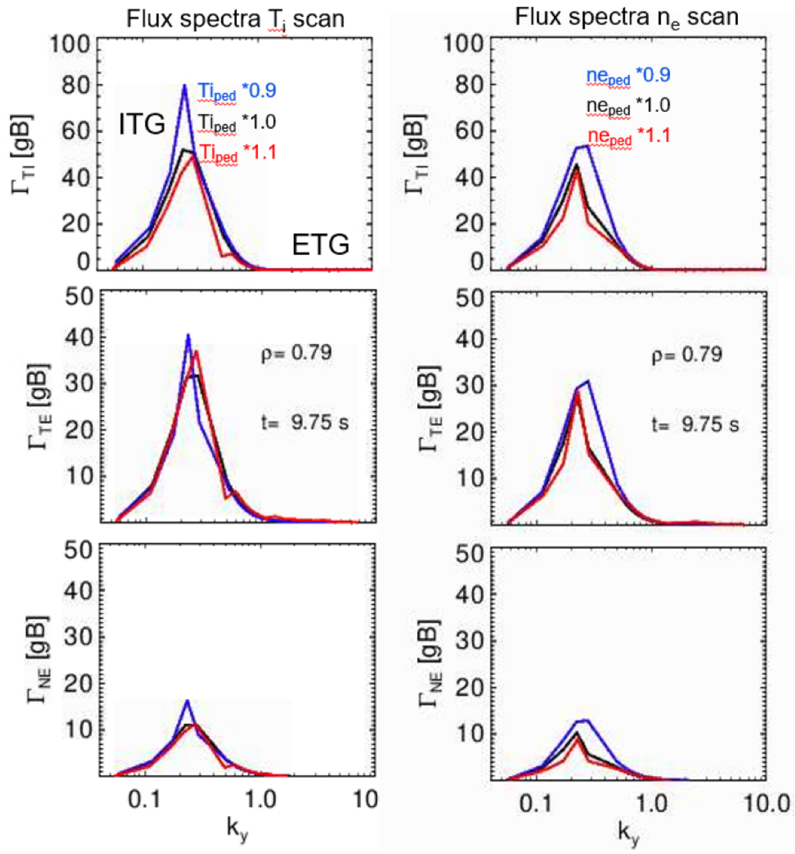

Figure 12. Quasi-linear flux spectra at $\rho_t = 0.79$ for the T_i scan (left column) and the n_e scan (right column). The colors refer to the the multiplying factor 0.9 (blue), 1.0 (black) and 1.1 (red) applied to the pedestal scanned quantity. From top to bottom, the spectra for ion flux, electron flux and particle flux are shown, highlighting how the larger T_i and density suppress the turbulence, respectively, on the ion heat channel and on the particle channel, respectively.

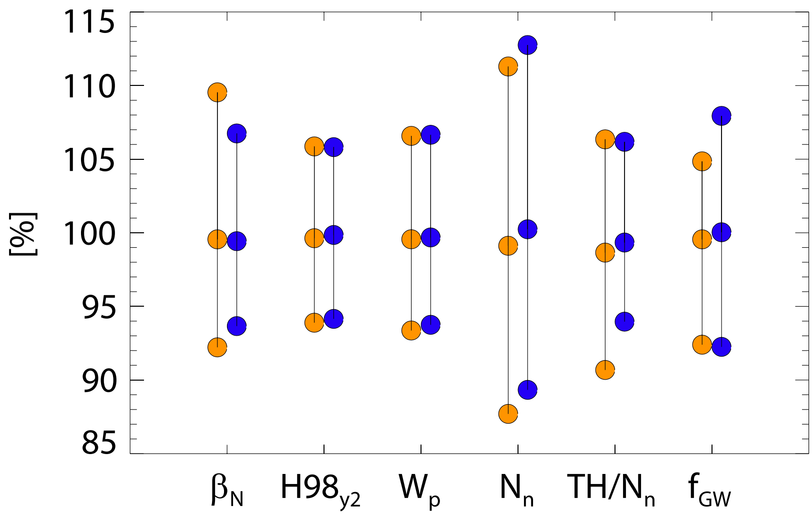

Figure 13. Variation interval of the plasma parameters characterizing the plasma performance. Minimum, average and maximum values obtained within the database are reported for each parameter, normalized to the reference simulations.

pedestal ion temperature propagates toward the core, and the ITG turbulence is decreased because of the larger T_i/T_e, damping, in particular, the particle fluxes (a symmetric effect is obtained by lowering the pedestal T_i). Also, the change in rotation and in rotation shear shows similar behaviors to the T_i modification: in this case, the dominant effect is on turbulence, since the pedestal kinetic profiles are not modified. A slightly more pronounced effect of the rotation shear modification is observed, in agreement with the turbulence suppression. The test on density provides only minor effects. This is due to the compensating behavior of transport and sources: while the transport is reduced ($n_e(0.85)\cdot 1.1$), the heat and particle sources are less penetrating the core, leading to lower kinetic profiles, and vice versa. The pedestal T_e variation provides only minor modification; indeed, also in this case, two opposite effects are present: the lower pedestal electron temperature is compensated by the reduced transport associated with larger T_i/T_e, leading to only minor differences in the modeled profiles. Finally, the Z effective sensitivity test has, at first sight, a peculiar behavior. The increased impurity content and dilution should lead to lower plasma performance. In the present modeling, an opposite outcome is obtained: the reason is that the increased dilution damps the turbulent fluxes, while it has no effects on the radiation power,introducing a small inconsistency in the prediction results of the Z_{eff} scan. Nevertheless such Z_{eff} scan with imposed radiation profile, isolates the effect of a measurement error on the Z effective used in the modeling: the measurement error on the Z_{eff} data has a non-negligible impact on the prediction results.

The turbulence suppression due to increased T_i and n_e, and to the reduced T_e is confirmed also by the quasi-linear spectra of the turbulent fluxes computed by TGLF for the 99 948 DT pulse, as reported in figure 12. In particular the larger T_i halves the transport of the ion heat component, whereas leaves unchanged the electron heat. Also the particle flux results slightly reduced. Also the dependence of the turbulence on the n_e levels is reported in the right column of figure 12: the larger pedestal density shows a positive effect on all the 3 channels investigated reducing the transport, but this is counterbalanced by the lower penetration of the beams: the 2 phenomena balance themselves producing no significant variation in the density and temperatures profiles.

The plasma performance variability in the whole database of simulations presented in table 1 is reported in figure 13: different performance indicator are reported, with their maximum, average, and minimum values normalized to the reference case. In such figure $\beta_N = \frac{<P_{tot}>_V}{B_t^2} 2\mu_0 \frac{aB_t}{I_p}$, where the plasma total pressure P_{tot} is volume averaged, the toroidal field B_t is taken at the plasma axis location, and $a = 0.5(R_{max} - R_{min})$ is the generalized minor radius at the mid plane. The confinement factor $H98_{y2}$ is taken from [24], W_p is the volume averaged total plasma stored energy, N_n is the total neutron rate, TH/N_n is the fraction of the neutron produced by thermonuclear reactions, and $f_{GW} = \frac{<n_e>_V}{I_p}\pi a^2$ is the Greenwald fraction. Comparing the variation intervals of each parameter of D and DT plasmas, no large differences are present. The neutron rate is the most sensitive parameter, featuring $\pm 15\%$ interval, whereas the stored energy (and $H98_{y2}$) are the least sensitive, with the variation or about $\pm 5\%$. This behavior can be explained by the fact that the neutron rate strongly scales with the ion temperature in the inner core, whereas volume integrated quantities are less sensitive. It's interesting to note that, in this scenario, the thermal neutron fraction accounts for about 50% of the total neutron rate, as confirmed also by its variation interval which turn out to be about half of the total neutron rate one.

5. Conclusion

The predictive modeling performed with TRANSP-TGLF in [5] showed a density under-prediction which affects both the baseline and the hybrid scenarios, in pure deuterium and in DT mixture. In this work we investigate the main reasons for such discrepancy identifying the lack of particle source as the main cause. The predictive modeling work done on the high-performance baseline pure deuterium pulse 96 482, with to a systematic optimization of the TRANSP-TGLF workflow and comparison with similar detailed calculation performed with JINTRAC, lead to the identification of an effective solution to mitigate the density under-prediction. The same optimized setup was then applied to the corresponding DT discharge 99 948, resulting in a good agreement with the experimental neutron rate, within 12%.

A sensitivity analysis on the main experimental inputs revealed that both the ion temperature T_i and the Z_{eff} exert the most significant influence on the predictive modeling results. This finding highlights the crucial importance of accurate measurements or assumptions for these quantities when attempting blind, first-principles predictions of DT plasma performance.

Overall, these results demonstrate that, once properly constrained, integrated modeling tools such as TRANSP-TGLF are capable of reliably extrapolating plasma behavior from D to DT conditions, providing a robust framework for scenario development and validation in support of future reactor-relevant operations.

Acknowledgments

The authors thank Dr Italo Predebon for useful discussions and support in the final revision of the manuscript. This work has been carried out within the framework of the EUROfusion Consortium, funded by the European Union via the Euratom Research and Training Programme (Grant Agreement No 101052200 EUROfusion). Views and opinions expressed are however those of the author(s) only and do not necessarily reflect those of the European Union or the European Commission. Neither the European Union nor the European Commission can be held responsible for them.

Appendix. List of TGLF settings

The detailed settings of TGLF switches used in the predictive modeling are indicated by table A1. The TGLF switches not indicated in table A1 were set by the default values, which can be found in https://gafusion.github.io/doc/tglf/tglf_table.html.

Table A1. List of the main TGLF switch settings used for the predictive simulations.

Switch	Definition	TRANSP
NS	No. kinetic species	4 (e,D,T,imp.)
GEOMETRY_FLAG_MODEL	1 = Miller geometry	1
USE_BPER	Include $\perp$ magnetic fluctuations	T
USE_BPAR	Include $\|$ magnetic fluctuations	F
SAT_RULE	Saturation rule	2
KYGRID_MODEL	4 = standard transport spectrum	4
NMODES	No. stored modes	6
NBASIS_MIN	Min. parallel basis functions	2
NBASIS_MAX	Max. parallel basis functions	6
NKY	No. high-k poloidal modes	19
ALPHA_MACH	Parallel velocity multiplier	0
ALPHA_E	$E \times B$ shear multiplier	1
ALPHA_QUENCH	0 = new spectral shift model	0
FILTER	Driftwave frequency threshold	2.0
USE_AVEION_GRID	Charge-avg. ρ_i for k_y grid	T

ORCID iDs

F. Auriemma 0000-0002-1043-1563
Hyun-Tae Kim 0009-0008-2549-5624
J. Lombardo 0009-0007-9349-0246
R. Lorenzini 0000-0001-8353-4857
S. Gabriellini 0000-0001-9488-5193
L. Garzotti 0000-0002-3796-9814
V.K. Zotta 0000-0002-3518-5178
M. Gorelenkova 0000-0001-8487-1396
F. Rimini 0009-0001-2917-0455
G.M. Staebler 0000-0002-1944-1733
Ž. Štancar 0000-0002-9608-280X
D. Van Eester 0000-0002-4284-3992
J. Garcia 0000-0003-0900-5564

References

[1] Garcia J. *et al* (JET Contributors) 2023 Modelling performed for predictions of fusion power in JET DTE2 overview and lessons learnt *Nucl. Fusion* **63** 112003
[2] Loarte A. *et al* 2025 The new ITER baseline, research plan and open R D issues *Plasma Phys. Control. Fusion* **67** 065023
[3] Maggi C.F. *et al* 2024 Overview of T and D-T results in JET with ITER-like wall *Nucl. Fusion* **64** 112012
[4] Stancar Z. *et al* (JET Contributors) 2023 Overview of interpretive modelling of fusion performance in JET DTE2 discharges with TRANSP *Nucl. Fusion* **63** 126058
[5] Hyun-Tae K. *et al* (JET Contributors) 2023 Validation of D–T fusion power prediction capability against 2021 JET D–T experiments *Nucl. Fusion* **63** 112004
[6] Garzotti L. *et al* (JET Contributors) 2025 Development of high-current baseline scenario for high deuterium-tritium fusion performance at JET *Plasma Phys. Control. Fusion* **67** 075011
[7] Pankin A.Y., Breslau J., Gorelenkova M., Andre R., Grierson B., Sachdev J., Goliyad M. and Perumpilly G. 2025 TRANSP integrated modeling code for interpretive and predictive analysis of tokamak plasmas *Comput. Phys. Commun.* **312** 109611
[8] Kinsey J.E., Staebler G.M. and Waltz R.E. 2008 The first transport code simulations using the trapped gyro-Landau-fluid model *Phys. Plasmas* **15** 055908
[9] Staebler G.M., Belli E.A., Candy J., Kinsey J.E., Dudding H. and Patel B. 2021 Verification of a quasi-linear model for gyrokinetic turbulent transport *Nucl. Fusion* **61** 116007
[10] Pasqualotto R., Nielsen P., Gowers C., Beurskens M., Kempenaars M., Carlstrom T. and Johnson D. (JET-EFDA Contributors) 2004 High resolution Thomson scattering for joint European torus (JET) *Rev. Sci. Instrum.* **75** 3891–3
[11] Frassinetti L., Beurskens M.N., Scannel R., Osborne T.H., Flanagan J., Kempenaars M., maslov M., Pasqualotto R. and Walsh M. (JET-EFDA Contributors) 2012 Spatial resolution of the JET Thomson scattering system *Rev. Sci. Instrum.* **83** 013506
[12] Schneider P.A. *et al* (JET Contributors) 2023 Isotope physics of heat and particle transport with tritium in JET-ILW type-I ELMy H-mode plasmas *Nucl. Fusion* **63** 112010
[13] Pankin A., McCune D., Andre R., Bateman G. and Kritz A. 2004 The tokamak Monte Carlo fast ion module NUBEAM in the National Transport Code Collaboration library *Comput. Phys. Commun.* **159** 157–84
[14] Tamor S. 1981 ANTIC: a code for calculation of neutral transport in cylindrical plasmas *J. Comput. Phys.* **40** 104–19
[15] Hahm T.S., Na D.H., Lee J.W., Park J.W., Na Y.S., Kim S.S., Ko W.H., Diamond P.H., Jhang H. and Jeon Y.M. 2013 E × B shear suppression of turbulence in diverted H-mode plasmas: role of edge magnetic shear *Nucl. Fusion* **53** 093005
[16] Burrell K.H. 2020 Role of sheared $E \times B$ flow in self-organized, improved confinement states in magnetized plasmas *Phys. Plasmas* **27** 060501
[17] Leoni C. *et al* 2024 Scrape-off layer opacity to D and T gas puff fuelling in JET baseline scenario *50th EPS Conf. on Plasma Physics* (*Salamanca, Spain, 8–12 July 2024*)
[18] Romanelli M. *et al* (EFDA-JET Contributors) 2014 JINTRAC: a system of codes for integrated simulation of tokamak scenarios *Plasma Fusion Res.* **9** 3403023
[19] Zotta V.K. *et al* (JET Contributors) 2022 Fusion power predictions for β N $\approx$ 1.8 baseline scenario with 50–50 D–T fuel mix and NBI injection in preparation to D–T operations at JET *Nucl. Fusion* **62** 076024
[20] Tala T. *et al* (JET Contributors) 2019 Density peaking in JET—determined by fuelling or transport? *Nucl. Fusion* **59** 126030

[21] Tala T. *et al* (JET Contributors) 2023 Isotope mass scaling and transport comparison between JET deuterium and tritium L-mode plasmas *Nucl. Fusion* **63** 112012
[22] Doyle E.J. *et al* (ITPA Transport Physics Topical Group, ITPA Confinement Database, Modelling Topical Group, ITPA Pedestal and Edge Topical Group) 2007 Chapter 2: plasma confinement and transport *Nucl. Fusion* **47** S18
[23] Citrin J. *et al* (JET-EFDA Contributors) 2014 Electromagnetic stabilization of tokamak microturbulence in a high-β regime *Plasma Phys. Control. Fusion* **57** 014032
[24] ITER Physics Basis Expert Groups on Confinement, Transport, Confinement Modeling and Database ITER Physics Basis editors 1999 Chapter 2: plasma confinement and transport *Nucl. Fusion* **39** 2175